

Self-Bondable and Stretchable Conductive Composite Fibers with Spatially Controlled Percolated Ag Nanoparticle Networks: Novel Integration Strategy for Wearable Electronics

Chaebien Kwon, Duhwan Seong, Jeongdae Ha, Dongwon Chun, Jee-Hwan Bae, Kukro Yoon, Minkyu Lee, Janghoon Woo, Chihyeong Won, Seungmin Lee, Yongfeng Mei, Kyung-In Jang, Donghee Son,* and Taeyoon Lee*

Advances in electronic textiles (E-textiles) for next-generation wearable electronics have originated from making a balance between electrical and mechanical properties of stretchy conductive fibers. Despite such progress, the trade-off issue is still a challenge when individual fibers are woven and/or stretched undesirably. Time-consuming fiber weaving has limited practical uses in scalable E-textiles. Here, a facile method is presented to fabricate ultra-stretchable Ag nanoparticles (AgNPs)/polyurethane (PU) hybrid conductive fibers by modulating solvent diffusion accompanied by in situ chemical reduction and adopting a tough self-healing polymer (T-SHP) as an encapsulation layer. First, the controlled diffusivity determines how formation of AgNPs is spatially distributed inside the fiber. Specifically, when a solvent with large molecular weight is used, the percolated AgNP networks exhibit the highest conductivity ($30\,485\text{ S cm}^{-1}$) even at 300% tensile strain and durable stretching cyclic performance without severe cracks by virtue of the efficient strain energy dissipation of T-SHP encapsulation layers. The self-bondable properties of T-SHP encapsulated fibers enables self-weavable interconnects. Using the new integration, mechanical and electrical durability of the self-bonded fiber interconnects are demonstrated while stretching biaxially. Furthermore, the self-bonding assembly is further visualized via fabrication of a complex structured E-textile.

1. Introduction

Fiber-based electronics comprise an emerging technology for the next generation of human-friendly wearable devices due to their superior flexibility, stretchability, and properties that can be easily integrated into clothes, which are coming from 1D configuration. The durable conductive fibers, the essential component for stable construction of fiber devices have been investigated with various materials and manufacturing methods. Commercially available conductive fibers are usually manufactured by applying metallic coatings to fibers. They exhibit excellent electrical conductivity, but their high moduli limits flexibility and stretchability.^[1–3] Alternatives including wires coated with conductive polymers and carbon nanotube (CNT) fibers, substitutes for metallic coatings, show poor performance such as relatively low electrical conductivity and inherent degradation under applied tensile strain.^[4–10] Thus, composite fibers comprised of polymers and conductive nanomaterials are currently in the

C. Kwon, K. Yoon, M. Lee, J. Woo, C. Won, S. Lee, Prof. T. Lee
Nanobio Device Laboratory
School of Electrical and Electronic Engineering
Yonsei University
50 Yonsei-ro, Seodaemun-gu, Seoul 03722, Republic of Korea
E-mail: taeyoon.lee@yonsei.ac.kr

D. Seong, Prof. D. Son
Department of Electrical and Computer Engineering
Sungkyunkwan University
2066 Seobu-ro, Jangan-gu, Suwon-si, Gyeonggi-do 16419
Republic of Korea
E-mail: daniel3600@g.skku.edu

 The ORCID identification number(s) for the author(s) of this article can be found under <https://doi.org/10.1002/adfm.202005447>.

J. Ha, Prof. K.-I. Jang
Department of Robotics Engineering
Daegu Gyeongbuk Institute of Science and Technology (DGIST)
333 Techno Jungang-daero, Hyeonpung-eup, Dalseong-gun
Daegu 42988, Republic of Korea

Dr. D. Chun, J.-H. Bae
Advanced Analysis Center
Korea Institute of Science and Technology (KIST)
5, Hwarang-ro 14-gil, Seongbuk-gu, Seoul 02792, Republic of Korea
Prof. Y. Mei
Department of Materials Science
Fudan University
Shanghai 200438, P. R. China

DOI: 10.1002/adfm.202005447

spotlight, because they remain highly electrically conductive when they undergo bending or twisting deformation.

The researches on the composite elastic fibers have been focused on uniform dispersion to ensure that conduction pathways remain stable under tensile strain.^[11–14] However, there is an obvious trade-off between stretchability and conductivity according to percolation theory; moreover, the modulus of a composite fiber increases when the additional conductive materials are added to enhance conductivity.^[15,16] Zhao et al. fabricated gold nanowires (AuNWs) embedded stretchable conductive fibers with dry spinning method.^[13] The AuNW-based fibers were conductive under tensile strain, but conductivity fell below 500 S cm^{-1} at 380% tensile strain, which can conclude that it is not enough to use as durable interconnectors in fiber devices under severe deformation conditions. To be durable, a conductive composite fiber must retain an electrical pathway and its polymeric properties by overcoming the percolation threshold.^[17] To this end, pre-strained conductive fibers with buckling structures have thus been developed to minimize the trade-off between stretchability and conductivity.^[13,18] Zhang et al. fabricated stretchable and conductive core-sheath fibers with buckled surfaces from pre-strained Lycra fibers and CNTs, then spray-coated them with silver nanowires (AgNWs).^[18] However, the conductivity of the fabricated fibers reached just 200 S cm^{-1} at 100% tensile strain, which indicated they would not be sufficiently durable for practical applications. Sunwoo et al. synthesized nanocomposites using Ag-Au core-shell nanowires and a polystyrene-butadiene-styrene (SBS) elastomeric block copolymer.^[19] They enhanced stretchability and conductivity by mixing Ag-Au nanowires with the elastomer and Pt black in optimal ratios. However, after optimizing the mass ratios of the base materials, an additional heat-rolling process was needed to obtain a highly stretchable and conductive nanocomposite. The lack of durable fiber-based interconnects to integrate fibrous components in supercapacitors,^[20–22] light-emitting devices,^[23–25] and energy generators,^[26–28] remains a technological barrier. Various researchers have investigated electrical components with 1D configurations. However, the ability to connect 1D components in fiber-based electronic devices using conventional textile integration methods, such as weaving, knitting, stitching, and embroidery is limited^[29–32] which has been an obstacle to the full integration and miniaturization of fiber-based devices.

Herein, ultra-stretchable surface-enriched Ag nanoparticles (AgNPs)/polyurethane (PU) hybrid conductive fiber which is encapsulated by tough self-healing polymers (T-SHPs) are presented as a fiber-based self-bondable and durable interconnects. The aqueous in situ reduction was used to control diffusivity of the solvent, which can control the concentration and position of the conductive nanomaterials and overcome the trade-off relationship between stretchability and conductivity. The hydroxyl solvent with larger molecular weights limited diffusivity,^[33] which enabled the outer AgNP shells and PU cores to locally segregate; Ag abundant conductive outer shell was formed while remaining pure polymeric characteristic core in fiber. Due to stable electrical pathways in highly dense Ag rich shell, the fiber exhibits the highest conductivity ($30,485 \text{ S cm}^{-1}$) even at 300% tensile strain. The fibers were encapsulated in a tough self-healing polymer (T-SHP) to prevent the propagation

of Ag rich shell cracks, the dominant factor of weakening percolated AgNPs networks. The T-SHPs coated fibers showed higher conductivity approximately 4 times than uncoated fibers during 1000 stretching cycles under 300% tensile strain. In addition, integration of fiber devices can be realized by utilizing T-SHPs which have self-bondable and easily attachable properties. The T-SHPs encapsulated stretchable conductive fibers can be employed as self-bondable and self-weavable interconnects, which is a new integration strategy for fiber-based devices. The self-bondable interconnects can be readily patterned, which circumvents the design constraints that have hobbled the development of fiber-based electronics. To prove our concept, light emitting diode (LED) was stably turned on with the help of the T-SHPs encapsulated stretchable conductive fiber. In addition, the complex structure of textile wolf tattoo was fabricated using the self-bonding assembly, showing it can be applied as an excellent and easily bondable interconnects.

2. Results and Discussion

Figure 1a i) shows an overall schematic illustration of the aqueous in situ chemical reduction method to fabricate the self-bondable (T-SHPs encapsulated) and stretchable conductive fiber. Commercially available spandex fibers were used as flexible matrices to make the stretchable conductive fibers. The magnified cross-sectional schematic demonstrates the swelling process on the aqueous in situ fabrication of the stretchable conductive fiber (**Figure 1a**). ii) The pure spandex matrices are illustrated with a yellow background and PU chains with hard segments and soft coiled segments are represented by the green lines. The soft coiled segments in the spandex fibers conferred elasticity, while the hard segments enabled them to retain their shape. The fabrication method involved two steps. In the first step, swelling enabled the fibers to absorb the Ag precursor solution. The Ag precursor in the fibers was then reduced by adding a hydrazine hydrate (N_2H_4) solution, resulting in the formation of AgNPs. Four different Ag precursor solutions containing 40 wt% AgCF_3COO each were prepared using methanol, ethanol, isopropyl alcohol (IPA), and butanol as solvents to study the effect of solvent molecular weight on diffusivity (**Figure 1a**). iii) Spandex fibers were immersed separately in the Ag precursor solutions for 20 min. As the spandex fibers swelled, ion-dipole interactions between trifluoroacetate anions (CF_3COO^-) and hydroxyl ($-\text{OH}$) groups in the solvent enabled the fibers to absorb the Ag precursor solution. The Ag precursor was expected to penetrate more deeply into the cores of the spandex fibers when it was dissolved in hydroxyl solvent with a low molecular weight. Thus, the depth to which the Ag precursor diffused into the spandex fiber was expected to follow the order methanol > ethanol > IPA > butanol. The experimental results shown in **Figure 2** confirmed this hypothesis. The stretchable conductive fibers were encapsulated in a T-SHP to make them self-bondable and attachable for application as durable interconnects.

Figure 1b presents AgNPs formation dominated by the molecular weight of hydroxyl solvents. The penetrated region of Ag precursor solution into the spandex fiber was indicated as pink color. The use of smaller molecular weight of hydroxyl solvents

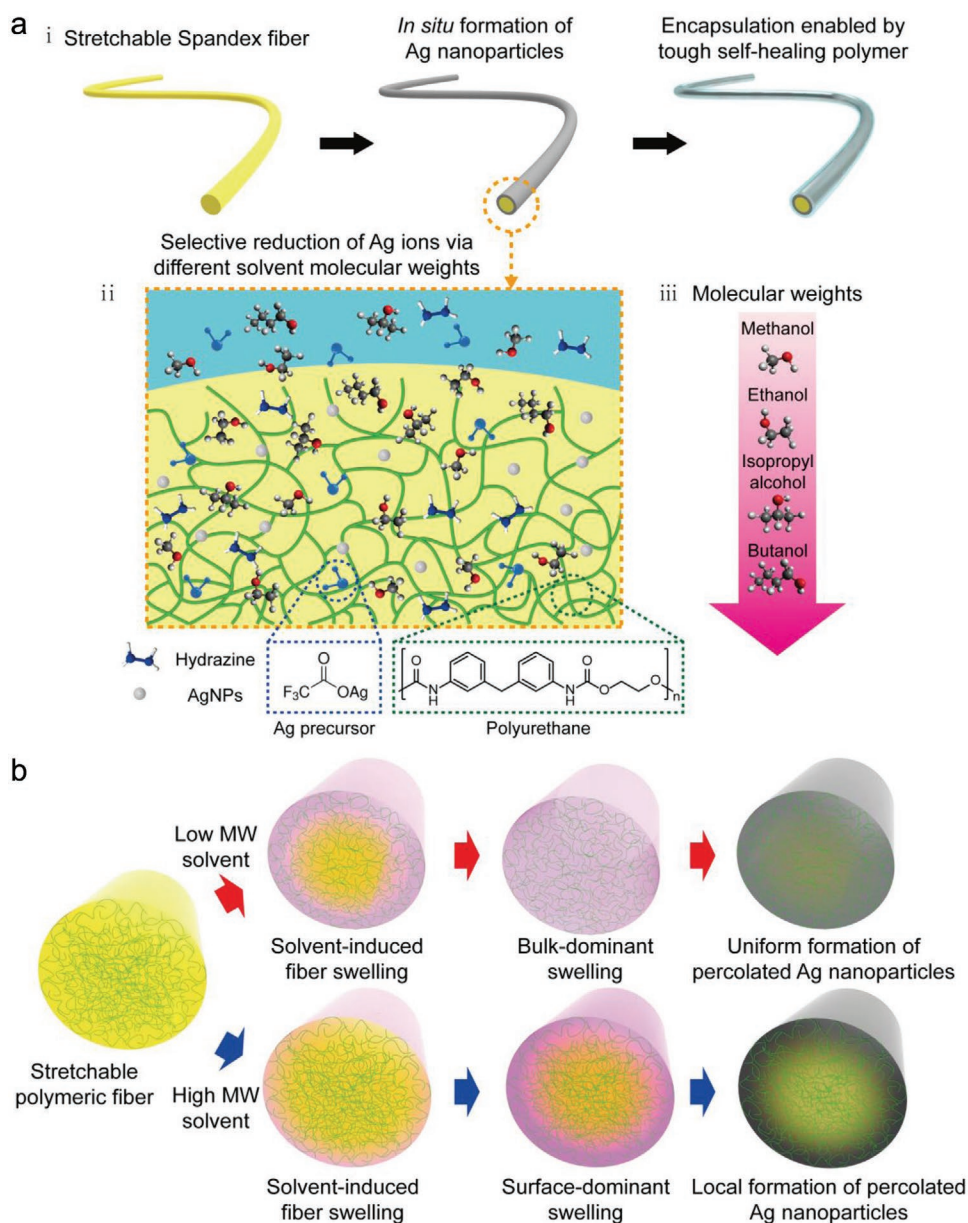


Figure 1. a) Schematic illustrations of i) *in situ* Ag nanoparticles (AgNPs) formation on a stretchable fiber and T-SHP encapsulation; ii) swelling and hydrazine reduction of the Ag precursor to obtain conductive stretchable fibers; iii) four hydroxyl solvents with different molecular weights. b) Tendency of AgNPs formation in hydroxyl solvents with different molecular weights (MWs).

was expected to allow Ag precursor to diffuse deep inside the spandex fiber, causing bulk-dominant swelling. The bulk-dominant swelling of Ag precursor may lead to uniform formation of AgNPs from outside to inside part of spandex fiber through the reduction. In contrast, the use of higher molecular weight of hydroxyl group solvents was expected to make Ag precursor permeates only at the outer periphery of the spandex fiber which can lead to surface-dominant swelling. The AgNPs shall be formed outside of the spandex fiber after reduction process if the Ag precursors penetrate only on the exterior part of the spandex fiber. The range in which the Ag precursor penetrates can be defined through diffusion control using different molecular weight of the hydroxyl group solvent. Remarkably,

mechanical and electrical performances of the stretchable conductive fiber are outstanding when the AgNPs were concentrated on the outer edge of the fiber, which will be discussed in more detail later.

Figure 2a,b show the Scanning Electron Microscope (SEM) plane and cross-view images of the butanol based stretchable conductive fiber, respectively, representing that the AgNPs are densely formed on the surface region of spandex fiber. Figure 2b notices the clear division between polymeric region and Ag-rich shell of the butanol based stretchable conductive fiber. The average Ag contents at four locations in 10 samples are plotted in Figure 2c. The Ag content obtained with each solvent was quantified by performing energy dispersive X-ray

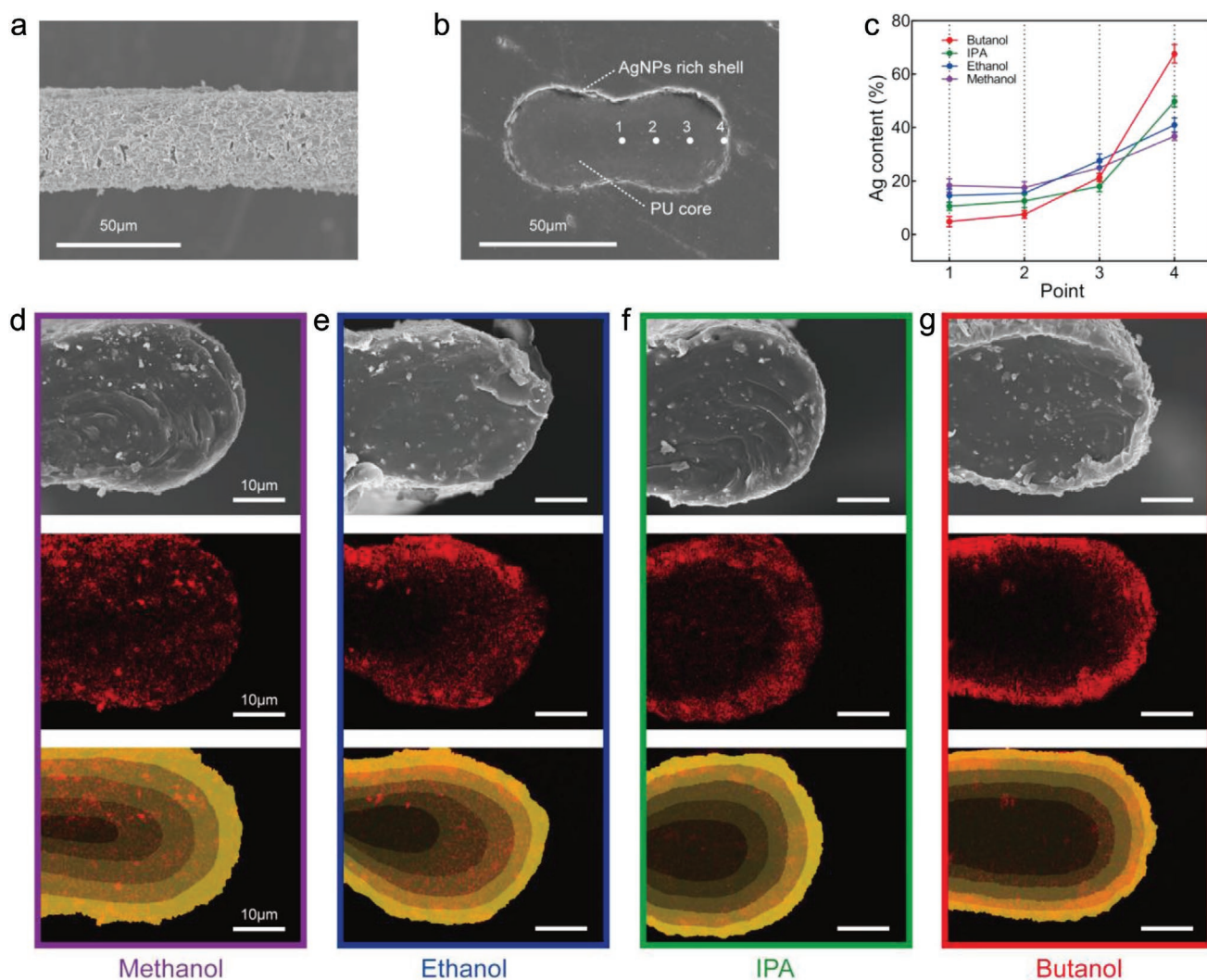


Figure 2. a) Planar SEM image of a butanol-based stretchable conductive fiber. b) Cross-sectional SEM image of a butanol-based stretchable conductive fiber. c) Ag contents measured at four points in stretchable conductive fibers fabricated using different solvents. d–g) Cross-sectional SEM images, EDS images, and contour maps of the various fibers with 20% concentration intervals.

spectroscopy (EDS) after one cycle of reduction. Points 1–4 in one of the samples are labeled in Figure 2b. Figure 2d shows the cross-sectional view of SEM, EDS images, and contour map of the methanol based stretchable conductive fiber. The EDS image indicates the AgNPs as red dots and shows that the AgNPs were formed gradually from outer regions to inside the fiber, which can be attributed to bulk-dominant swelling process in aqueous in-situ reduction. The bottom contour map indicates every 20% concentration intervals, obtained by image-analyzing program, Image area. Figure 2e–g show the cross-sectional view of SEM, EDS images, and contour map of the ethanol, IPA, and butanol based stretchable conductive fiber, respectively. With increasing molecular weight of solvent in fiber fabrication, the pure polymeric regions became larger due to limited penetration of the Ag precursor. The layers in the contour map of the fiber obtained using butanol were thinner (Figure 2g), since AgNPs are densely formed on the outside of the fiber due to surface-dominant swelling process, leading

the stretchable conductive fibers to have distinctive regions; an AgNPs rich outer shell and a polymeric core of the fibers.

Figure 3a exhibits the force of each hydroxyl solvent-based stretchable conductive fibers against tensile strain every 100% up to 500%. All fibers show mechanical hysteresis with different loading and unloading paths indicated as arrows. The front part of the loop under large strain does not overlap with the loop under small strain completely. This is due to the slow loading and unloading speed ($\approx 4 \text{ mm s}^{-1}$) which is the factor of time-dependent behavior on the strain of viscoelastic material.^[34] A viscoelastic material relaxes over time, which results in a small loop. We noted that the butanol solvent fiber has the most similar mechanical hysteresis loop with a pristine spandex fiber (indicated red line and dashed black line in Figure 3a, respectively). The force required to stretch each fiber to 500% tensile strain followed the order 0.15957 N (methanol) > 0.14162 N (ethanol) > 0.13620 N (IPA) > 0.09704 N (butanol) > 0.09693 N (pristine spandex). The

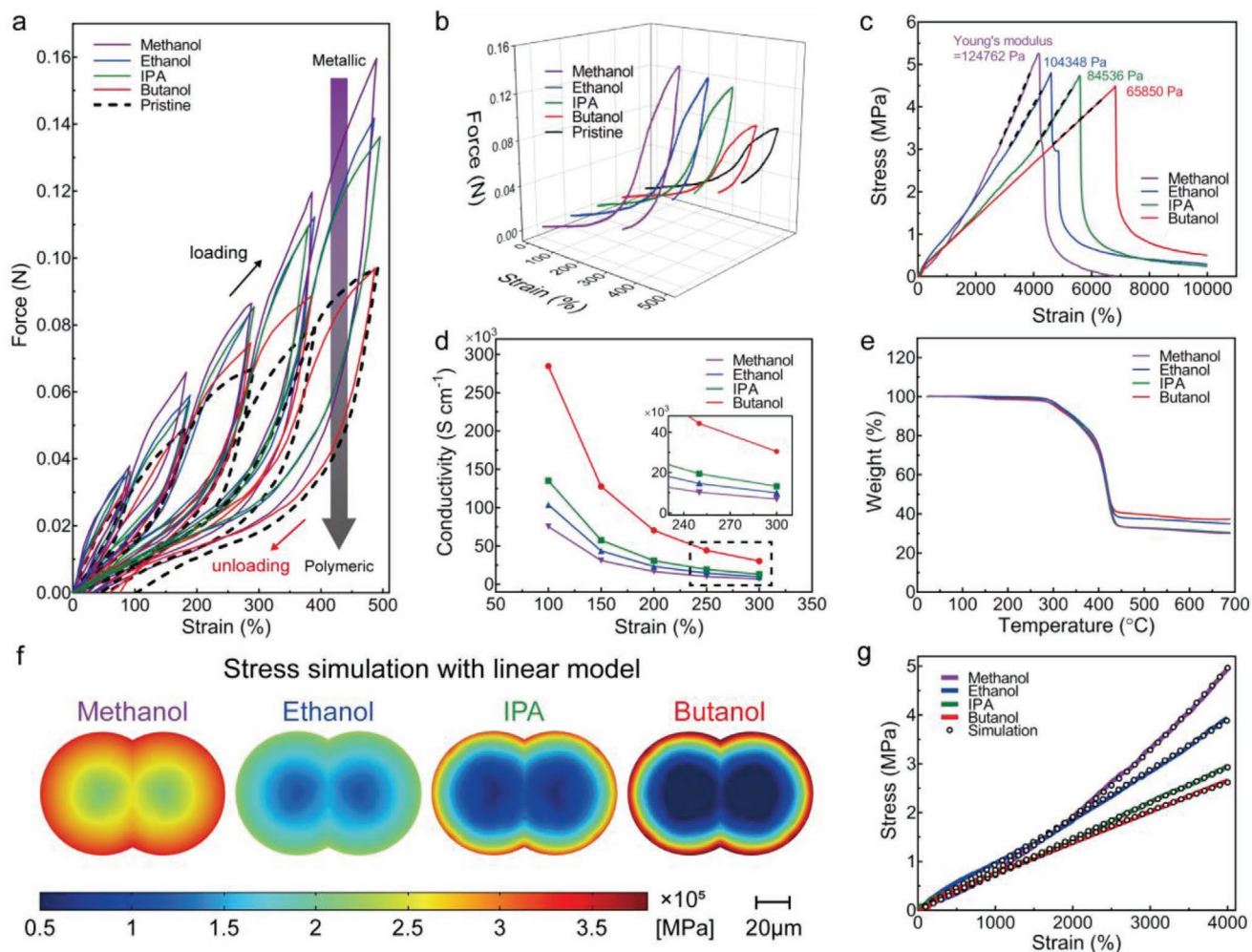


Figure 3. a) Force of stretchable conductive fibers fabricated using various solvents and a pristine spandex fiber at tensile strains of 100% to 500%. b) 3D plots of five different force loops under 500% tensile strain. c) Stress of the stretchable conductive fibers under tensile strain. d) Conductivity of the stretchable conductive fibers under tensile strain. e) Weight (%) of AgNPs in the stretchable conductive fibers determined via thermogravimetric analysis (TGA). f) Stress under 4,000% tensile strain simulated using a linear model. g) Comparison of experimental and simulated stress values.

large amount of force required to stretch the fiber obtained using methanol can be attributed to a relative metallic characteristic of the stretchable conductive fiber owing to the uniform distribution of AgNPs. On the contrary, in the higher molecular weight solvent case, the entire fiber exhibits polymeric property, segregating outer AgNPs-rich shell and PU core as pure. The strain-force loops of the stretchable conductive fibers under 500% tensile strain were replotted in a triple-axis graph (Figure 3b) to clearly visualize each loop. Figure 3c indicates the strain-stress curve of each stretchable conductive fiber up to the mechanical fracture. The methanol solvent fiber had the largest Young's modulus, approximately 124 762 Pa and early fracture occurred at 4,160% tensile strain. Young's modulus decreased as the molecular weight of the solvent increased. Young's modulus of butanol solvent fiber was reduced to 65,850 Pa and fracture occurred at 6,812% tensile strain, which is in good accordance with the results of Figure 3a. Figure 3d shows the conductivity of each fiber against tensile strain up to 300%. Interestingly, despite its polymeric mechanical properties, the fiber obtained using

butanol as a solvent exhibited the highest conductivity at an overall tensile strain of 300%. Figure 3e indicates the weight percentages of AgNPs with varying solvents obtained by thermo-gravimetric analysis (TGA). Although the weights of AgNPs in the fibers obtained using methanol and butanol differed by only $\approx 7\%$, the conductivity of the butanol-based fiber was remarkably high at 300% tensile strain, revealing tendency that overcomes trade-off relationship between stretchability and conductivity (see Figure 3c,d). Figure 3f is the stress simulation data under 4,000% tensile strain based on linear model. COMSOL Multiphysics 5.5 was used to analyze the distribution of stress in the conductive fibers based on the finite element method. A mixed solid Guth-Gold model was used for finite element analysis.^[35] According to this model, Young's modulus is a quadratic function of the AgNPs volume fraction. The swelling penetration depth of silver depended on the molecular weight of the solvent, which is an important factor of location and volume fraction of AgNPs. For the sake of simplicity, the simulation was performed assuming the actual shape and size of the monofilament matched those

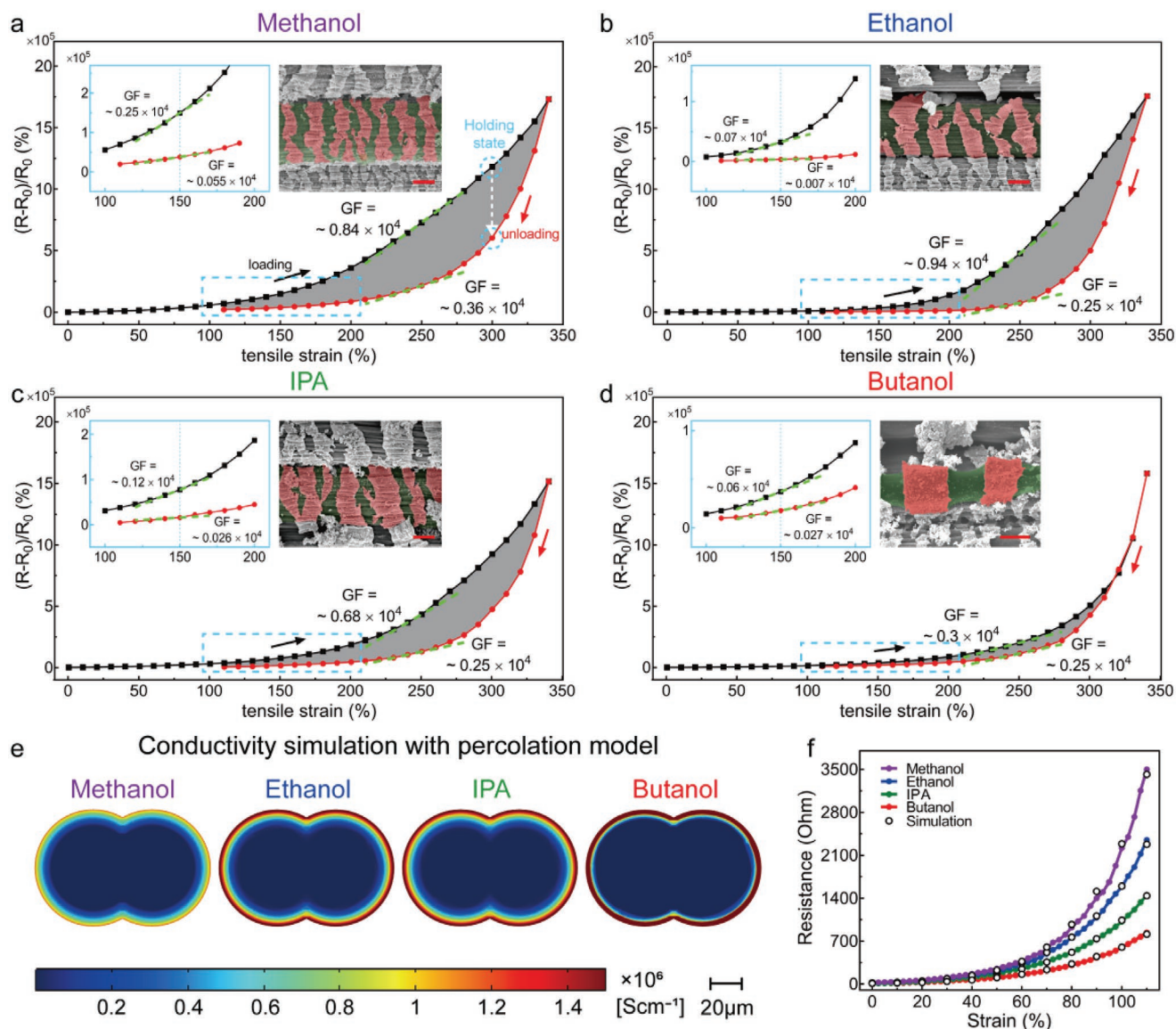


Figure 4. a–d) Relative changes in the resistance of stretchable conductive fibers under tensile strain. Insets: GFs of the dense Ag-rich shells (red) and polymeric regions (green) of fibers obtained using methanol, ethanol, IPA, and butanol (scale bar = 10 μm). e) Simulated conductivity values for fibers under 110% tensile strain based on the percolation model. f) Comparison of experimental and simulated resistance values.

of the fiber shown in Figure 2b. A similar trend in stress was observed in the simulations, even if the number of filaments was increased. The monofilament was assumed to have the shape of two combined cylinders. Colors in the images reflect the amount of stress in cross sections of the stretchable conductive fibers at 4,000% tensile strain. The stress of methanol solvent fibers in which AgNPs are formed gradually inside the fiber is range from 2.3×10^5 MPa to 3.5×10^5 MPa, indicating an overall high stress values. On the other hand, in the case of butanol solvent fibers, where AgNPs are concentrated in the outer part of the fiber, the stress of inner part was lower than 0.5×10^5 MPa and the stress of outer part was over 3.5×10^5 MPa. This explains that abundant formation of AgNPs on the periphery of the fiber help stretchable conductive fiber to endure a high range of tensile strain, maintaining

remarkable stretchability. Figure 3g indicates that the experimental stress values are consistent with simulation results.

Figure 4a–d indicate the relative changes in the resistance as a function of tensile strain for each stretchable conductive fiber. Hysteresis was nearly absent in the plot of the conductive fiber fabricated using butanol (see gray marked area). We noted the reason for the difference between loading and unloading paths. For the case of methanol solvent fiber at 300% tensile strain, relative changes in the resistance was $11.83 \times 10^5\%$ under loading process and decreased to $6.04 \times 10^5\%$ under unloading process. We assumed that the relative changes in the resistance decreased due to polymeric core rearrangement and viscoelasticity of the composite fiber. Time elapsed between the loading and unloading processes, because resistance was measured after allowing the fibers to rest for 60 s between each 10%

increase tensile strain. In fact, resistance actually decreased over time to the value of unloading when stretching was on hold (see the sky blue dashed arrow at 300% tensile strain in Figure 4a). During the time intervals, polymer link reconstruction occurs, resulting in decrease of resistance. The conductive pathways in stretchable fibers are generally located in the dense AgNP-rich shells and AgNPs embedded in the polymeric cores. The relatively small contribution of the polymeric cores of the fibers fabricated using butanol to conduction resulted in low hysteresis. Interestingly, the butanol solvent fiber showed highest conductivity under tensile strain among the fibers. The modified percolation theory for multifilament structures could explain the excellent conductivity of the fiber.^[17] The Ag-rich shell was the predominant factor in maintaining stable conduction pathways.^[36] To investigate the effect of Ag-rich shell, the outer shell of the fiber was cracked under 100% tensile strain (inset of Figure 4a–d). The size of the cracks varied with the solvent. The average width of the cracks increased from 5.22 μm to 6.36 μm , increased again to 8.09 μm , and finally increased to 11.91 μm as the molecular weight of the solvent increased. Moreover, surface dominant swelling process increased the density of AgNPs in the shell region in the butanol solvent fiber, which was confirmed by TGA in Figure 3e. Although the butanol solvent fiber has a large gap between cracked shells and fewer AgNPs embedded polymeric core, 3D modified percolation model in multifilament structure complements the fore-mentioned factors, with maintaining more contacts between the neighboring Ag-rich shells, enhancing stability of the conductive pathway. Figure 4e shows the conductivity simulation data of each stretchable conductive fiber under 110% tensile strain. The conductivities of each solvent-based fiber were calculated using percolation theory. The volume of silver in the microvolume of each fiber (V_f) was calculated based on percolation theory

$$V_f = \frac{\gamma V_{ag0}}{\int \gamma dV} \quad (1)$$

$$\sigma = (V_f - V_{c0})^s \quad (2)$$

$$\sigma = \left(\frac{\gamma V_{ag0}}{\int \gamma dV} - V_{c0} \right)^s + \sigma_f (V_f - V_{c0} > 0) \quad (3)$$

$$\sigma = \sigma_f (V_f - V_{c0} < 0) \quad (4)$$

V_f is the volume fraction of silver and γ is the mass ratio of silver and pure fiber. V_{ag0} is the total volume of silver in the fiber and V_{c0} is threshold volume fraction in percolation theory. σ_f is the conductivity of pure fiber and σ is the conductivity of conductive fiber. The theoretical resistance of the stretchable conductive fiber was approached by substituting the derived conductivity in to Ohm's law.

$$R = \frac{L}{\int \sigma dA} = \frac{L_0(1+\epsilon)}{\int \sigma dA} \quad (5)$$

The derivation of conductivity and resistance based on percolation theory are described in Equation S1, Supporting

Information. Conductivity in the range from 0.2×10^6 to $1.4 \times 10^6 \text{ S cm}^{-1}$ is indicated by color in Figure 4e. The predominant electron conduction pathways were present in the Ag-rich shells, and the fiber fabricated using butanol had the densest AgNPs shell. It can be seen that the conductive path is concentrated on the outer edge of the fiber from the simulation image of the butanol solvent fiber. Figure 4f indicates that the experimental resistance values are consistent with simulation results. The experimental resistance values shown in Figure 4f were consistent with the simulation results. To use the fibers as stretchable interconnects, differences between the gauge factors (GFs) during loading and unloading had to be small. The electrical stability of the butanol solvent fiber as interconnect can be demonstrated by the small numerical differences between loading and unloading GF at 150% and 250% tensile strain. The loading GF and unloading GF at 150% tensile strain were 0.06×10^4 and 0.027×10^4 , respectively, showing little difference (Figure 4d inset). Furthermore, at 250% tensile strain, the loading GF and unloading GF were 0.3×10^4 and 0.25×10^4 , representing stable electrical performance compared with other solvent-based stretchable conductive fibers (Figure 4d).

Although there have been significant improvements in the stretchability and conductivity of spatially controlled AgNP networks supported on elastic PU spandex fibers, their mechanical durability is still problematic. Uncontrolled crack propagation resulting in non-uniform electrical percolation pathways is a persistent challenge, because an optimal strategy to efficiently dissipate strain has not been developed. To make the relatively rigid Ag networks more deformable, a tough self-healing elastomer (T-SHP) comprising dynamic multivalent hydrogen bonds based on molecular steric hindrance was used to encapsulate the fibers. It could withstand extreme stretching and notch-induced crack propagations through its high toughness^[37] (Figure 5a). The Ag networks in the T-SHP matrix may have also enabled the autonomous repair of broken percolation pathways owing to the free volume created by the deformed T-SHP.^[38,39] To investigate this hypothesis, we stretched an encapsulated conductive fiber fabricated using butanol up to 300% strain (Figure 5b). Resistance varied little at strains ranging from 0% to 200%. Subsequent two- to four-fold increases were minor. Its electrical performance was slightly degraded under extreme strains in the range from 200% to 300%. However, such deformation is not expected for textile-based wearable electronics under normal conditions, because the strain of epidermal deformation does not exceed $\approx 30\%$.^[40] The T-SHP encapsulation layer on the PU spandex fiber shown in Figure 5b (inset) did not delaminate when the fiber was stretched up to 300% strain. This indicated that the interface between the T-SHP layer and the Ag network/PU fiber was robust. Hydrogen bond formation and efficient dissipation of strain energy had effects that were similar to those of a previously reported tough adhesion strategy.^[41] To quantify improvements in the T-SHP encapsulated fiber, we measured resistance in a pristine fiber and an encapsulated fiber during stretching (Figure 5c). As expected, the normalized resistance values of the encapsulated fiber were remarkably lower than those of the pristine fiber. The cyclic stretching result of Figure 5d followed nearly identical trends compared to that of Figure 5c. These experimental data clearly supported our assumptions about

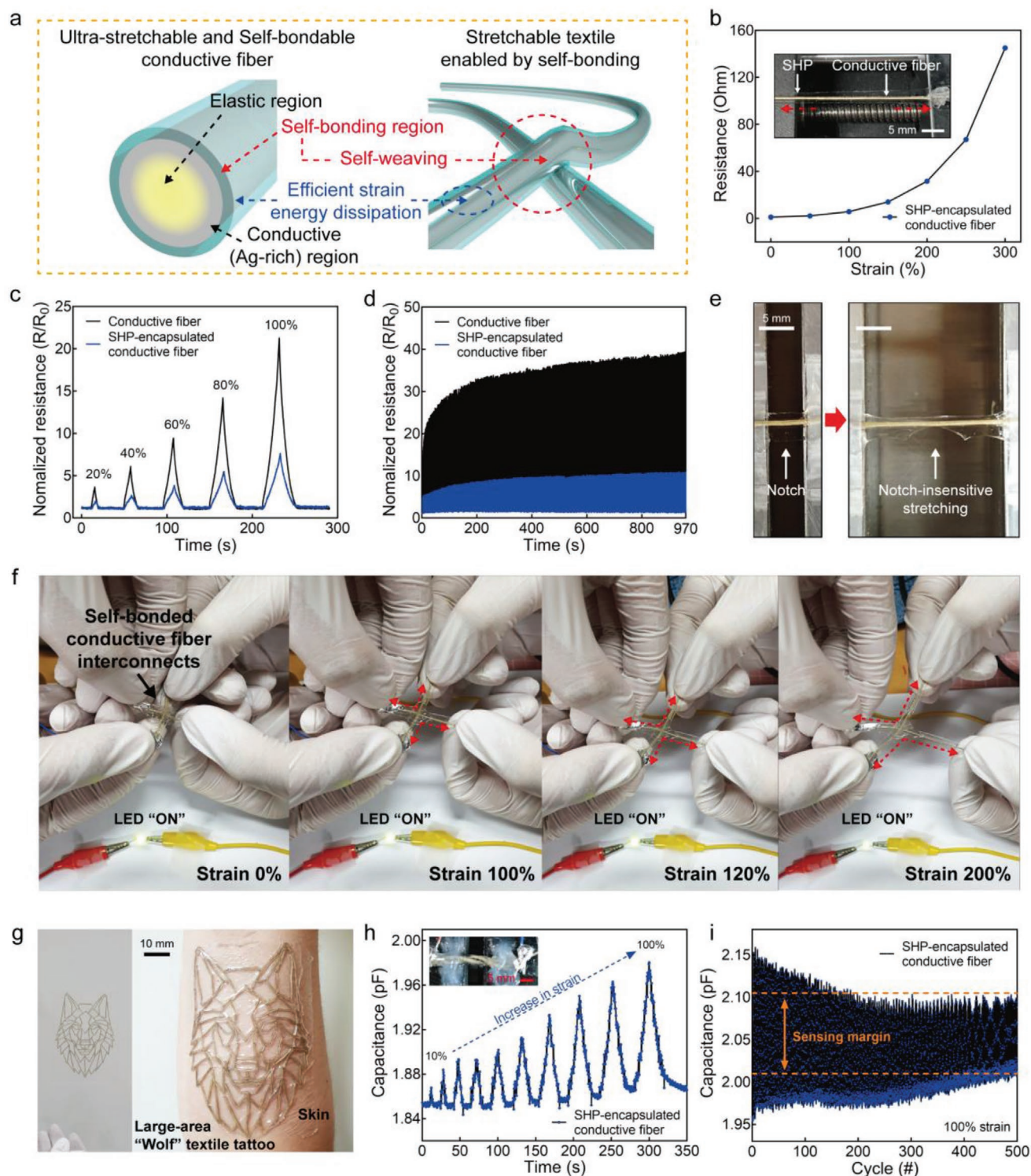


Figure 5. a) Schematic cross-sectional illustrations of a T-SHP-encapsulated conductive fiber (left) and two self-bonded conductive fibers (right). b) Resistance and strain characteristics of the encapsulated fibers stretched up to 300% strain. c) Changes in the normalized resistance of a conductive fiber (black) and a T-SHP-encapsulated conductive fiber (blue) as a function of time under strains of 20%, 40%, 60%, 80%, and 100%. d) Cyclic stretching durability of a conductive fiber (black) and a T-SHP-encapsulated conductive fiber (blue). e) Notch-insensitive stretching performance of the T-SHP-encapsulated conductive fiber. f) The electrical performance of two self-bonded conductive fibers stretched up to 200% strain. g) Photograph showing a large textile tattoo of a wolf on skin. h) Real-time measurements of strain sensor capacitance. The inset shows the helical structure of the capacitive strain sensor. i) Cyclic stretching durability of the capacitive strain sensor.

the effects of T-SHP encapsulation. In addition to its electrical properties, multivalent hydrogen bonds in the T-SHP enabled the conductive fiber to endure damage (Figure 5e). An encapsulated conductive fiber was notched and stretched at a tensile strain exceeding 400%, and undesired crack propagation was effectively suppressed. This may have been due to the high degree of T-SHP toughness, which originated from the complementary strong and weak bonding effect of the T-SHP.

Textiles are usually fabricated by weaving individual fibers, because sewing can mechanically damage the fibers. The self-healing effect of the T-SHP can be viewed as a unique breakthrough that circumvents this challenge for the realization of next-generation textile electronics (Figure 5a, right). The two encapsulated conductive fibers shown in Figure 5f and Movie S1, Supporting Information, self-bonded in the perpendicular direction without any external optical or thermal stimulus. The electrical performance of the self-bonded conductive fibers remained stable when they were stretched up to 200% strain. As a simple demonstration, we fabricated a complex structure of large-scale textile tattoo using the self-bonding assembly (Figure 5g). Such a scalable demonstration fully supports our new materials strategy in textile electronic applications. In this regard, we were able to fabricate a stretchable capacitive strain sensor composed of two twisted fibers. As such, the twisted spiral structure improves mechanical reversibility.^[42] As expected, our sensor reliably sensed strain and exhibited good cyclic stretching endurance (Figure 5h,i; Movie S2, Supporting Information). If the T-SHP encapsulation strategy combines with Au shell coating, our self-bondable and stretchable conductive composite fiber would be widely used for future bioelectronic devices.^[43]

3. Conclusion

We fabricated self-bondable and stretchable conductive composite fibers that could be used as interconnects for wearable electronics using a facile in situ chemical reduction process. The AgNP density was effectively controlled by varying the molecular weight of the Ag precursor solvent. Surface swelling in fibers fabricated using butanol as the Ag precursor solvent resulted in clear local segregation of the AgNP outer shells and the PU cores. An Ag-rich conductive outer shell formed, while the core retained the properties of a pure polymer. Due to the stability of electrical pathways in the Ag-rich shells, this type of fiber exhibited excellent conductivity ($30\ 485\ \text{S cm}^{-1}$) under 300% tensile strain. In addition, due to the pure polymeric characteristic of inner parts of the fiber, butanol solvent fiber showed broad tensile range with fracture occurrence at 6,812%. The fibers were encapsulated with a T-SHP to prevent crack propagation in the Ag-rich shells. Crack propagation in percolated AgNPs networks is the predominant cause of weakening. As expected, the T-SHP layer improved the electrical and mechanical durability of the encapsulated fibers. In addition, the T-SHP encapsulation enabled the formation of self-bondable and self-weavable fiber interconnects. This is a new integration strategy for the fiber-based multifunctional electronic devices. The self-bonding interconnects can be patterned easily, which removes design constraints as technical challenges to the development of the electronic textiles. We could reproducibly

turn on a LED using the encapsulated fibers, and fabricated a complex structure of textile wolf tattoo, which demonstrated that they could be applied as effective and readily patternable interconnects.

4. Experimental Section

Synthesis of the Self-Healing Polymer: The self-healing polymer was synthesized using a previously reported method. Polydimethylsiloxane with aminopropyl terminal groups (100 g, Gelest, DMS-A21) was dissolved in chloroform, and triethylamine (10 mL, TCI, T0424) was added at 0 °C under N₂ atmosphere. Methylene bis(phenyl isocyanate) (0.4 eq, TCI, D0897) and isophorone diisocyanate (0.6 eq, TCI, I0314) were added dropwise. The mixture was stirred for four days at room temperature. The polymer was precipitated by adding methanol and chloroform, then dried. For all experiments, the dried SHP (3 g) was dissolved in chloroform, poured into Teflon dish, and dried.

Fabrication of the SHP Encapsulated Butanol-based Stretchable Conductive Fibers: Creora Power Fit polyurethane-based spandex fibers were purchased from Hyosung and used as base materials for the stretchable conductive fibers. An Ag precursor solution was prepared by mixing AgCF₃COO (40 wt%) and butanol, and the fibers were soaked in the solution for 20 min to allow them to absorb the Ag precursor. The butanol was allowed to evaporate from the spandex fibers for 5 min, and the Ag nanoparticles were obtained via chemical reduction using 1:1 (v/v) hydrazine hydrate in ethanol as a reducing agent. After reducing the Ag precursor for 3 min, the fibers were rinsed several times with deionized (DI) water to remove any remaining hydrazine hydrate and allowed to dry. Also, the fibers fabricated using methanol, ethanol, and ipa were produced in the same way. The T-SHP was then used to encapsulate the conductive fibers. The fibers were heated at 70 °C for 30 min to accelerate the self-healing process.

Characterization: A 7610FPlus field emission scanning electron microscope (FE-SEM, JEOL, Japan) was used to obtain cross-sectional images and EDS of the stretchable conductive fibers. Cracks in the Ag shells were examined using a JSM-IT500HR FE-SEM (JEOL). TGA was performed to measure the amount of Ag in the fibers using a Q50 thermal analyzer (TA Instruments). The distribution of Ag nanoparticles was analyzed using the 7610FPlus FE-SEM and Image J software. A B2901A source meter (Keysight Technologies, USA) and an S2M force transducer (HBM, USA) were used to investigate the mechanical and electrical properties of the fibers. Simulated stress and conductivity results were obtained using COMSOL Multiphysics 5.5 (COMSOL, USA). The cyclic stretching test was conducted using a customized deformation analysis system with a motorized X-translation stage (Jaeil Optical Corp., Korea). A 2450 source meter (Keithley, USA) was used to monitor resistance in the stretchable conductive fibers. The capacitance of the strain sensor was measured using a 4284A precision LCR meter (Agilent, USA).

Supporting Information

Supporting Information is available from the Wiley Online Library or from the author.

Acknowledgements

C.K. and D.S. contributed equally to this work. This research was supported by the National Research Foundation of Korea (NRF) funded by Ministry of Science and ICT (NRF-2017M3A7B4049466, NRF-2020R1C1C1005567), Priority Research Centers Program through the National Research Foundation of Korea (NRF-2019R1A6A1A11055660), and Yonsei-KIST Convergence Research Program (NRF-2019R1A6A1A11055660). D.S. provided informed consent prior to mounting the textile tattoo onto his skin.

Conflict of Interest

The authors declare no conflict of interest.

Keywords

fiber component integration, self-bondable conductive fibers, stretchable and flexible interconnects, wearable electronics

Received: June 29, 2020

Revised: July 28, 2020

Published online:

- [1] S. Zhu, J. H. So, R. Mays, S. Desai, W. R. Barnes, B. Pourdeyhimi, M. D. Dickey, *Adv. Funct. Mater.* **2013**, *23*, 2308.
- [2] Y. Bian, R. Liu, X. Huang, J. Hong, H. Huang, S. Hui, *Smart Mater. Struct.* **2015**, *24*, 105001.
- [3] J. Feng, M. Sun, J. Li, X. Liu, S. Jiang, *Anal. Chim. Acta* **2011**, *701*, 174.
- [4] L. Allison, S. Hoxie, T. L. Andrew, *Chem. Commun.* **2017**, *53*, 7182.
- [5] J. Eom, R. Jaisutti, H. Lee, W. Lee, J. S. Heo, J. Y. Lee, S. K. Park, Y. H. Kim, *ACS Appl. Mater. Interfaces* **2017**, *9*, 10190.
- [6] M. P. Prabhakaran, L. Ghasemi-Mobarakeh, G. Jin, S. Ramakrishna, *J. Biosci. Bioeng.* **2011**, *112*, 501.
- [7] Y. S. Chiam, K. S. Lim, S. W. Harun, S. N. Gan, S. W. Phang, *Sens. Actuators, A* **2014**, *205*, 58.
- [8] X. Zhang, Q. Li, Y. Tu, Y. Li, J. Y. Coulter, L. Zheng, Y. Zhao, Q. Jia, D. E. Peterson, Y. Zhu, *Small* **2007**, *3*, 244.
- [9] W. Li, F. Xu, W. Liu, Y. Gao, K. Zhang, X. Zhang, Y. Qiu, *Composites, Part A* **2018**, *108*, 107.
- [10] W. Weng, Q. Sun, Y. Zhang, H. Lin, J. Ren, X. Lu, M. Wang, H. Peng, *Nano Lett.* **2014**, *14*, 3432.
- [11] J. R. Bautista-Quijano, P. Pötschke, H. Brünig, G. Heinrich, *Polymer* **2016**, *82*, 181.
- [12] Q. Tian, Z. Xu, Y. Liu, B. Fang, L. Peng, J. Xi, Z. Li, C. Gao, *Nanoscale* **2017**, *9*, 12335.
- [13] Y. Zhao, D. Dong, S. Gong, L. Brassart, Y. Wang, T. An, W. Cheng, *Adv. Electron. Mater.* **2019**, *5*, 1800462.
- [14] S. W. Kim, S. N. Kwon, S. I. Na, *Composites, Part B* **2019**, *167*, 573.
- [15] D. Ren, S. Zheng, F. Wu, W. Yang, Z. Liu, M. Yang, *J. Appl. Polym. Sci.* **2014**, *131*, 39953.
- [16] H. J. Choi, M. S. Kim, D. Ahn, S. Y. Yeo, S. Lee, *Sci. Rep.* **2019**, *9*, 6338.
- [17] J. Lee, S. Shin, S. Lee, J. Song, S. Kang, H. Han, S. Kim, S. Kim, J. Seo, D. Kim, T. Lee, *ACS Nano* **2018**, *12*, 4259.
- [18] Y. Zhang, W. Zhang, G. Ye, Q. Tan, Y. Zhao, J. Qiu, S. Qi, X. Du, T. Chen, N. Liu, *Adv. Mater. Technol.* **2020**, *5*, 1900880.
- [19] S.-H. Sunwoo, S. I. Han, H. Kang, Y. S. Cho, D. Jung, C. Lim, C. Lim, M.-J. Cha, S.-P. Lee, T. Hyeon, D.-H. Kim, *Adv. Mater. Technol.* **2020**, *5*, 1900768.
- [20] G. Qu, J. Cheng, X. Li, D. Yuan, P. Chen, X. Chen, B. Wang, H. Peng, *Adv. Mater.* **2016**, *28*, 3646.
- [21] J. Ren, L. Li, C. Chen, X. Chen, Z. Cai, L. Qiu, Y. Wang, X. Zhu, H. Peng, *Adv. Mater.* **2013**, *25*, 1155.
- [22] Z. Yang, J. Deng, X. Chen, J. Ren, H. Peng, *Angew. Chem., Int. Ed.* **2013**, *52*, 13453.
- [23] S. Kwon, W. Kim, H. Kim, S. Choi, B. C. Park, S. H. Kang, K. C. Choi, *Adv. Electron. Mater.* **2015**, *1*, 1500103.
- [24] H. Zheng, Z. Zhang, S. Jiang, B. Yan, X. Shi, Y. Xie, X. Huang, Z. Yu, H. Liu, S. Weng, A. Nurmikko, Y. Zhang, H. Peng, W. Xu, J. Zhang, *Nat. Commun.* **2019**, *10*, 2790.
- [25] X. Zhou, X. Xu, Y. Zuo, M. Liao, X. Shi, C. Chen, S. Xie, P. Zhou, X. Sun, H. Peng, *J. Mater. Chem. C* **2020**, *8*, 935.
- [26] Z. Wen, M. H. Yeh, H. Guo, J. Wang, Y. Zi, W. Xu, J. Deng, L. Zhu, X. Wang, C. Hu, L. Zhu, X. Sun, Z. L. Wang, *Sci. Adv.* **2016**, *2*, E1600097.
- [27] X. He, Y. Zi, H. Guo, H. Zheng, Y. Xi, C. Wu, J. Wang, W. Zhang, C. Lu, Z. L. Wang, *Adv. Funct. Mater.* **2017**, *27*, 1604378.
- [28] T. Chen, L. Qiu, Z. Yang, Z. Cai, J. Ren, H. Li, H. Lin, X. Sun, H. Peng, *Angew. Chem., Int. Ed.* **2012**, *51*, 11977.
- [29] L. Wang, L. Wang, Y. Zhang, J. Pan, S. Li, X. Sun, B. Zhang, H. Peng, *Adv. Funct. Mater.* **2018**, *28*, 1804456.
- [30] K. Dong, Y. C. Wang, J. Deng, Y. Dai, S. L. Zhang, H. Zou, B. Gu, B. Sun, Z. L. Wang, *ACS Nano* **2017**, *11*, 9490.
- [31] Y. E. Shin, J. E. Lee, Y. Park, S. H. Hwang, H. G. Chae, H. Ko, *J. Mater. Chem. A* **2018**, *6*, 22879.
- [32] L. Zhang, T. Andrew, *Adv. Electron. Mater.* **2018**, *4*, 1800271.
- [33] W. Hayduk, W. D. Buckley, *Chem. Eng. Sci.* **1972**, *27*, 1997.
- [34] B. J. Yang, B. R. Kim, H. K. Lee, *Compos. Struct.* **2012**, *94*, 1420.
- [35] E. Guth, *Phys. Rev.* **1938**, *53*, 322.
- [36] M. Park, J. Im, M. Shin, Y. Min, J. Park, H. Cho, S. Park, M. B. Shim, S. Jeon, D. Y. Chung, J. Bae, J. Park, U. Jeong, K. Kim, *Nat. Nanotechnol.* **2012**, *7*, 803.
- [37] J. Kang, D. Son, G. J. N. Wang, Y. Liu, J. Lopez, Y. Kim, J. Y. Oh, T. Katsumata, J. Mun, Y. Lee, L. Jin, J. B. H. Tok, Z. Bao, *Adv. Mater.* **2018**, *30*, 1706846.
- [38] N. Matsuhisa, D. Inoue, P. Zalar, H. Jin, Y. Matsuba, A. Itoh, T. Yokota, D. Hashizume, T. Someya, *Nat. Mater.* **2017**, *16*, 834.
- [39] S. H. Kim, H. Seo, J. Kang, J. Hong, D. Seong, H. J. Kim, J. Kim, J. Mun, I. Youn, J. Kim, Y. C. Kim, H. K. Seok, C. Lee, J. B. H. Tok, Z. Bao, D. Son, *ACS Nano* **2019**, *13*, 6531.
- [40] D.-H. Kim, N. Lu, R. Ma, Y.-S. Kim, R.-H. Kim, S. Wang, J. Wu, S. M. Won, H. Tao, A. Islam, K. J. Yu, T.-I. Kim, R. Chowdhury, M. Ying, L. Xu, M. Li, H.-J. Chung, H. Keum, M. McCormick, P. Liu, Y.-W. Zhang, F. G. Omenetto, Y. Huang, T. Coleman, J. A. Rogers, *Science* **2011**, *333*, 838.
- [41] J. Li, A. D. Celiz, J. Yang, Q. Yang, I. Wamala, W. Whyte, B. R. Seo, N. V. Vasilyev, J. J. Vlassak, Z. Suo, D. J. Mooney, *Science* **2017**, *357*, 378.
- [42] T. N. Do, Y. Visell, *Sci. Rep.* **2017**, *7*, 1753.
- [43] S. Choi, S. I. Han, D. Jung, H. J. Hwang, C. Lim, S. Bae, O. K. Park, C. M. Tschabrunn, M. Lee, S. Y. Bae, J. W. Yu, J. H. Ryu, S.-W. Lee, K. Park, P. M. Kang, W. B. Lee, R. Nezafat, T. Hyeon, D.-H. Kim, *Nat. Nanotechnol.* **2018**, *13*, 1048.